Progress In Electromagnetics Research, Vol. 165, 119–130, 2019

Uniform Beamwidth UWB Feed Antenna Using Lossy Transmission Lines

Carl Pfeiffer[1, *], Thomas Steffen[1], and George Kakas[2]

Abstract—The ideal ultra-wideband (UWB) antenna feed for lens and reflector systems radiates a uniform and customizable beamwidth vs. frequency. Here, a new antenna concept for radiating frequency-independent Gaussian beams with arbitrary bandwidths and beamwidths is reported. It is analytically shown how to resistively load a transmission line network to maintain a Gaussian amplitude taper across an antenna array aperture. In contrast to many other feed antennas, the radiation properties here can be tailored without time-consuming full wave optimizations. The radiated beamwidth, bandwidth, antenna size, radiation efficiency, and gain can all be quickly estimated using the derived closed-form expressions. An example, 16×16 Vivaldi element array is fed with a network of resistively loaded microstrip lines. The simulated array radiates a Gaussian beam with 10 dB full beamwidth of $35^\circ \pm 5^\circ$ and directivity of 20 dB $\pm$ 1.5 dB over 6.5 GHz–19 GHz (3 : 1 bandwidth ratio). However, the radiation efficiency is inherently low due to the large loss associated with generating the Gaussian amplitude taper at all frequencies. The example array has a simulated radiation efficiency of 1% at the higher operating frequencies. The array was fabricated and measured. The measured beamwidths agree well with simulation to validate the reported theory. This architecture is a particularly attractive option for feed antennas that require customizable directivities, and can tolerate low radiation efficiencies such as test and measurement.

1. INTRODUCTION

Test and measurement systems often use lenses and reflectors to shape electromagnetic fields (e.g., compact reflector antenna measurements, free space material measurements, free space S-parameter measurements). These systems commonly employ corrugated horns as sources since they radiate a Gaussian beam with high mode purity [1]. This allows system engineers to use simple quasi-optical formulas to design the location, focal lengths, and diameters of various quasi-optical components [2]. However, these horns only operate over the waveguide bandwidth (less than one octave). Ultra-wideband measurements therefore require swapping feed horns across the different bands. Alignment and calibration steps need to be performed every time the feed horn is replaced, which is time consuming and expensive. This motivates the use of UWB feed antennas. The ideal feed maintains a constant radiation pattern vs. frequency. However, it can be challenging to realize such an antenna since the vast majority of directive antennas have a beamwidth that reduces with frequency due to the increased electrical size of the aperture.

Antennas radiating frequency-independent radiation patterns have been extensively studied. Flared horn antennas can realize stable patterns over multi-octave bandwidths [3, 4]. However, they require extensive design optimization and are quite bulky. Furthermore, they can have relatively high peak cross-pol levels of -10 dB [4]. The dual stacked log-periodic antenna uses a two element array of log

Received 12 August 2019, Accepted 15 September 2019, Scheduled 9 October 2019
* Corresponding author: Carl Pfeiffer (carlpfei@umich.edu).
[1] Defense Engineering Corporation, 2458 Dayton Xenia Rd, Beavercreek, OH 45434, USA. [2] Air Force Research Laboratory, Sensors Directorate, 2241 Avionics Circle Wright-Patterson Air Force Base, USA.

periodic antennas to improve the H-plane directivity over that of a single log-periodic antenna. These antennas maintain a near-constant directivity of $\sim 10\,\text{dB}$ over a decade bandwidth. A similar concept is employed in the Eleven antenna [5], which also realizes a constant beamwidth over a decade, good impedance match, and high radiation efficiency. However, extensive optimization is required to properly tune the antenna dimensions. In addition, the peak cross-polarized radiation is only $-10\,\text{dB}$ down in some cases [6]. Sinuous antennas have also been designed to have a similar performance [7]. It is unclear how to modify the design of these log-periodic based antennas for applications requiring directivities higher than $\sim 10\,\text{dB}$. An UWB design with substantially higher directivity was reported in [8]. This antenna employs a leaky wave slot between two different dielectrics to realize frequency independent radiation at mm-wave frequencies. However, there is asymmetry between the E and H planes, as well as high sidelobe levels. The highest performance option is to utilize an active electronically scanned phased array (AESA) since every element has a phase shifter and attenuator that can be calibrated across all operating frequencies [9]. Thus, AESAs can realize optimal radiation patterns over ultra-wide operational bandwidths. However, they are complicated and expensive.

Here, a new concept for a UWB, passive antenna array is reported that realizes a near-constant directivity over a bandwidth of 6.5 to 19 GHz. The array is fed with a network of lossy transmission lines whose insertion loss increases with frequency to compensate for the increased electrical size of the aperture at higher frequencies. A systematic design process is reported which allows the array to be easily scaled for nearly arbitrary radiated beamwidths. The simple design procedure comes at the cost of low radiation efficiency at high frequencies though. Therefore, it is envisioned this antenna is only useful for UWB test and measurement applications where lower signal strengths can be better tolerated. Simulations show good agreement with theory. A 16×16 element Vivaldi antenna array is designed with a simulated 10 dB full beamwidth of $35^\circ \pm 5^\circ$ over the operating band. The array is fabricated and measured. The measured beamwidths agree well with calculations. However, the measured radiation patterns do have large sidelobes due to unexpected radiation from the microstrip feed network. A method to eliminate this unwanted radiation in future antennas is discussed.

2. IDEAL GAUSSIAN BEAM SOURCE

Gaussian beams are commonly utilized in quasi-optical systems since they can be easily controlled with high precision using lenses and mirrors. At the location of beam waist ($z = 0$), an ideal Gaussian beam has an electric field profile ($E(r, \lambda)$) given by,

$$E\left(r,\lambda\right) = e^{-\frac{r^2}{w_0^2(\lambda)}} \tag{1}$$

where $r = \sqrt{x^2 + y^2}$ is the radial distance from the beam axis; w_0 is the beam waist radius; and λ is the free space wavelength. The normalized far field radiated by the beam ($E_{ff}(\theta, \lambda)$) is given by the Fourier transform of the field profile,

$$E_{ff}\left(\theta,\lambda\right) = \iint E\left(r,\lambda\right) e^{j\left(\frac{2\pi}{\lambda}\right)\sin(\theta)(x+y)} dxdy = e^{-\left(\frac{\sin(\theta)\pi w_0(\lambda)}{\lambda}\right)^2} \tag{2}$$

where θ is the angle from the beam axis. Therefore, the beam waist radius must be directly proportional to the wavelength for realizing a frequency independent far field. Combining Eqs. (1) and (2) gives the ideal field profile at the aperture of the antenna for realizing a Gaussian beam with constant beamwidth vs frequency,

$$E\left(r,\lambda\right) = e^{-\left(\frac{r\pi\sin(\theta_0/2)}{\lambda}\right)^2} \tag{3}$$

where θ_0 is the full beamwidth at which the power drops to $1/e^2$ (8.7 dB).

Consider an antenna array fed with an ideal UWB corporate power divider as shown in Figure 1. The corporate power divider is assumed to be lossless for now. Lossy transmission lines that function as frequency dependent attenuators connect the power divider outputs to the radiating elements. From Eq. (3), we can immediately draw some conclusions on the performance limitations using this resistive taper approach. First, the Gaussian beam mode purity is analyzed. Since an ideal Gaussian amplitude distribution extends to infinity, it must be truncated at some point. The Gaussian beam coupling

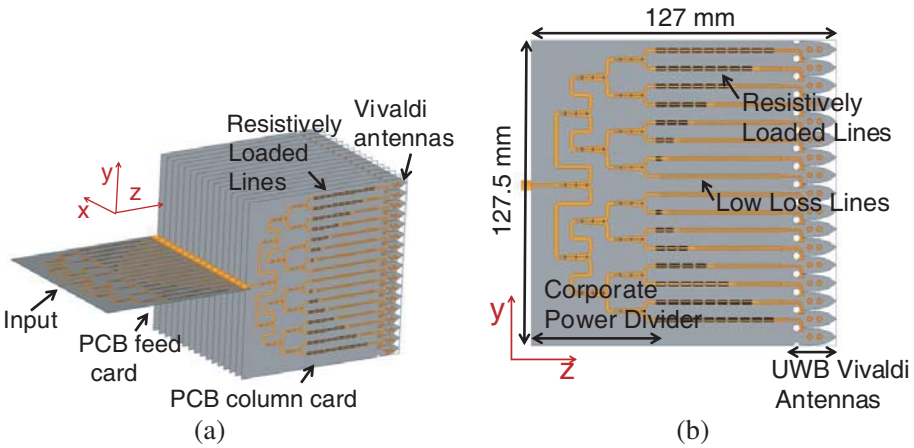

Figure 1. (a) UWB Vivaldi antenna array fed with a lossy transmission line network for realizing uniform beamwidth vs. frequency. (b) PCB column card that consists of a corporate power divider, lossy transmission line network, and UWB radiating elements. The microstrip lines are represented by the orange traces, while the dark grey sections represent the ground plane/Vivaldi radiators.

coefficient (e_{coup}) quantifies the mode purity and is defined as the inner product of the field at the aperture and that of an ideal Gaussian beam [2]. It is straightforward to show that the coupling coefficient is equal to

$$e_{coup}\left(r_{ap},\lambda\right)=1-e^{-2\left(\frac{r_{ap}\pi\sin(\theta_0/2)}{\lambda}\right)^2} \tag{4}$$

where r_{ap} is the antenna aperture's radius. Since the antenna employs attenuation to realize the Gaussian amplitude taper, the radiation efficiency (e_{rad}) is another important performance metric. Taking the ratio of the power available from the corporate power divider to the total power at the aperture gives the radiation efficiency,

$$e_{rad}\left(r_{ap},\lambda\right)=\frac{\lambda^2 e_{coup}}{2r_{ap}^2\pi^2\sin^2\left(\theta_0/2\right)} \tag{5}$$

For a given operating wavelength, a larger antenna aperture radius (r_{ap}) leads to a higher Gaussian mode purity (e_{coup}), but a lower radiation efficiency (e_{rad}). Let us define the maximal operating wavelength ($\lambda_{\max}$) to be such that the beam waist radius is equal to the antenna radius. In this case, the aperture size is related to the beamwidth by

$$r_{ap}=\lambda_{\max}/(\pi\sin\left(\theta_0/2\right)) \tag{6}$$

In this case, the coupling coefficient and radiation efficiency are 86% and 43%, respectively, at the largest operating wavelength. The wavelength dependence on the radiation efficiency (5) simplifies to,

$$e_{rad}\left(r_{ap},\lambda\right)=\frac{1}{2}\left(\frac{\lambda}{\lambda_{\max}}\right)^2\left(1-e^{-2\left(\frac{\lambda_{\max}}{\lambda}\right)^2}\right)=\frac{1}{2}\left(\frac{\lambda}{\lambda_{\max}}\right)^2 e_{coup} \tag{7}$$

Equation (7) illustrates that there is a clear tradeoff between bandwidth and radiation efficiency. For example, the radiation efficiency at the highest operating frequency must be less than 0.5% for an antenna with a 10 : 1 bandwidth ratio. Note that the coupling efficiency is very near 100% at the highest operating frequencies for wideband antennas, in accordance with Eq. (4).

Next, a physical implementation of this lossy transmission line network is discussed. An idealized lossy parallel plate transmission line shown in Figure 2(a) is first considered because it has a simple analytic model that provides physical intuition for understanding the basic concepts. A more practical microstrip implementation will be discussed in the sections that follow. The parallel plate waveguide consists of a stackup of air and a lossy dielectric characterized by conductivity σ, which are sandwiched between two perfectly conducting plates on the top and bottom. Assuming the parallel plate thickness

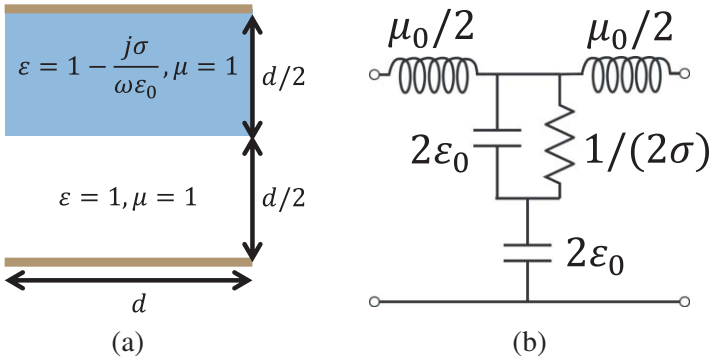

Figure 2. (a) Parallel plate waveguide loaded with a lossy dielectric. (b) Circuit model for the parallel plate transmission line.

is much less than the wavelength in all materials, the quasi-TEM transmission line mode can be modeled with the equivalent circuit shown in Figure 2(b). The line has an effective permittivity given by [10],

$$\varepsilon_{eff} = 2\frac{(1 - j\sigma/(\omega\varepsilon_0))}{(2 - j\sigma/(\omega\varepsilon_0))} \tag{8}$$

Furthermore, assuming that the lossy material acts as a good conductor ($\sigma/(\omega\varepsilon_0) \gg 1$), the effective refractive index is simplified to,

$$n_{eff} = \sqrt{\varepsilon}_{eff} = \sqrt{2}\,(1 - j\omega\varepsilon_0/(2\sigma)) \tag{9}$$

and the field along the transmission line behaves as,

$$E\,(z, \lambda) = \exp\,(-jz\omega n_{eff}/c) = \exp\left(\frac{-jz\omega}{c}\sqrt{2}\right)\exp\left(\frac{-z2\sqrt{2}\pi^2\varepsilon_0 c}{\lambda^2\sigma}\right) \tag{10}$$

where exp denotes exponential; $c = 1/\sqrt{\varepsilon_0\mu_0}$ is the speed of light in free space; and z is the position along the transmission line. Note that the assumption of a good conductor ($\sigma/(\omega\varepsilon_0) \gg 1$) is equivalent to assuming the lines have a low insertion loss per wavelength. Comparing Eq. (3) with Eq. (10), the resistively loaded transmission line can realize the necessary amplitude taper for generating the desired far field, provided that the transmission line lengths ($l_{lossy}(r)$) satisfy,

$$l_{lossy}(r) = \frac{r^2\sigma\lambda_{\max}^2}{2\sqrt{2}\pi^2 r_{ap}^2 c\varepsilon_0} = \frac{r^2\lambda_{\max}^2}{\sqrt{2}\pi r_{ap}^2\lambda}\left(\frac{\sigma}{\omega\varepsilon_0}\right) \tag{11}$$

The required length of each transmission line feed is a function of the radial distance from the beam axis (r), material loss (σ), and maximum operating wavelength ($\lambda_{\max}$). Since l_{lossy} is not a function of frequency, it is possible to design an aperture with arbitrary bandwidth ratio that radiates a pure Gaussian beam at all frequencies. However, there exists some practical limitations. Long transmission lines are required for wide bandwidths ($\lambda_{\max}/\lambda_{\min} \gg 1$). For example, an array with a $10:1$ bandwidth ratio employing a high conductivity material ($\sigma/(\omega\varepsilon_0) > 10$) requires transmission lines that are $100\lambda_{\max}/(\sqrt{2}\pi) = 22\lambda_{\max}$. In practice, the requirement of high σ (i.e., low insertion loss/wavelength) can be relaxed somewhat to reduce the required antenna size without significantly sacrificing performance. However, reducing σ too much leads to unwanted dispersion that makes it challenging to provide wideband phase matching.

It is also important to note that the lossy transmission lines have an elevated real part of the refractive index (i.e., phase delay) compared to free space (see Eq. (9)). Here, the real part of the refractive index is $\sqrt{2}$ when the lossy material thickness and the free space thickness are identical, as shown in Figure 2(a). This fact is important since the transmission line network feeding the array consists of a combination of high-loss and low-loss line segments to realize a Gaussian amplitude taper with uniform phase. It is important that the low-loss transmission lines are engineered to have an identical phase velocity as the high loss segments to ensure every line is phase matched.

It should be emphasized that although the parallel plate waveguide is not used in the following sections, it offers simple analytic expressions for understanding several aspects of the array. For example, a lossy transmission line with the equivalent circuit shown in Figure 2(b) can generate the exact frequency dependent insertion loss that is desired for realizing a frequency-independent beamwidth. The loss leads to an elevated real part of the refractive index. Increasing the line's attenuation reduces the necessary feed network depth (i.e., antenna size). But the loss cannot be too large since the transmission line lengths should be on the order of $\lambda_{\max}^2/\lambda_{\min}$ to ensure they are not too dispersive. The lossy transmission line lengths should increase quadratically from the center towards the outside.

3. DESIGN AND SIMULATION

3.1. Lossy Transmission Lines

A prototype antenna is designed. The lossy parallel plate waveguide discussed in the previous section provides a simple and intuitive analytic model for understanding some of the basic concepts. However, the parallel plate transmission line is not the most practical line from a fabrication standpoint. Therefore, a microstrip transmission line with the same equivalent circuit as the parallel plate waveguide is designed (see Figure 2(b)). The lossy microstrip lines have dimensions shown in Figure 3(a). Microstrip lines are chosen because they can be fabricated using low-cost printed-circuit-board (PCB) techniques. In addition, integrating resistive loading is straightforward using screen printed carbon ink. An important feature of the parallel plate waveguide circuit model (see Figure 2(b)) is the resistance in series with the capacitance to ground. This series resistance is implemented here using a $100\,\Omega$/sq carbon loaded resistive ink patterned on the copper signal traces. Current flows from the signal trace, through the resistive ink, and through a capacitance to ground.

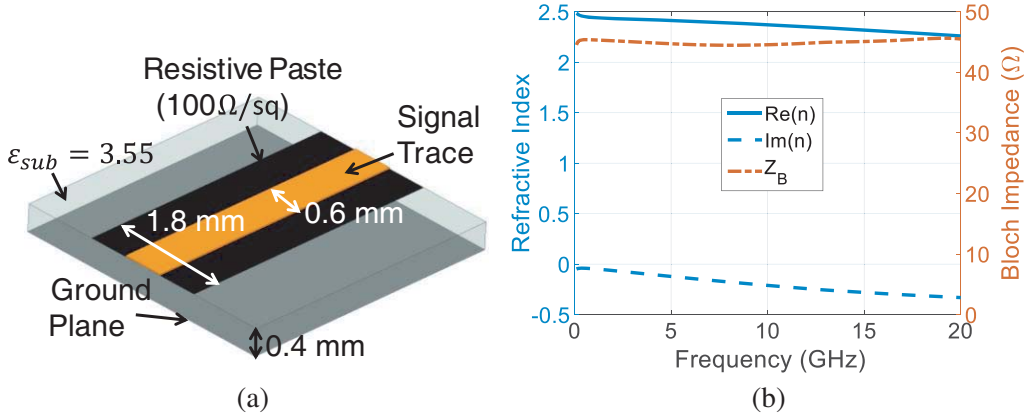

Figure 3. (a) Lossy microstrip line loaded with $100\,\Omega$/sq resistive paste. (b) Refractive index and Bloch impedance of the lossy microstrip line.

The Bloch impedance and refractive index of the lossy transmission line are shown in Figure 3(b). They are calculated using S-parameters of the transmission line from ANSYS HFSS [11]. The lines have a $45\,\Omega$ impedance, $\mathrm{Re}(n_{eff}) = 2.4$, and $\mathrm{Im}(n_{eff})$ that decreases nearly linearly from 0 to -0.35 as the frequency varies from 0 to 20 GHz. The imaginary part of the index is then combined with Eq. (9) to calculate an effective material conductivity $\sigma_{eff} = 2.3\,\mathrm{S/m}$ so that the parallel plate waveguide design rules can be applied. This effective conductivity is inserted into (11) to calculate the required lengths of the lossy transmission lines as a function of position in the array, where the minimum operating frequency is 6.5 GHz. Note that there is some unwanted line dispersion since $\mathrm{Re}(n_{eff})$ decreases from 2.4 to 2.2 when the frequency changes from 1 GHz to 19 GHz. This negative dispersion is due to the fact that the attenuation constant is quite high to reduce the required line lengths ($\sigma/(\omega\varepsilon_0) > 2.2$) Line dispersion affects the phase uniformity at the aperture. Simulations suggest that there is less than 45° phase variation across the radiating aperture for all operating frequencies.

It can be inferred from Eq. (11) that the design is robust to variance in the resistive ink properties, which can be challenging to precisely control in practice. For fixed geometrical parameters, the resistivity of the ink is proportional to the radiated beamwidth squared ($\sin^2(\theta_0/2)$). For example, if the paste resistivity increases by 20% due to fabrication tolerances, the beam shape is unchanged and the beamwidth increases by only 10%.

3.2. Phase Matching with Low-Loss Transmission Lines

The field at the array aperture should have a uniform phase. Since the lossy transmission lines have variable lengths, low loss lines need to be added to realize a planar aperture with uniform phase. The low-loss lines require an identical $\mathrm{Re}(n_{eff})$ as the lossy lines. However, it was shown earlier that resistive loading necessarily increases the effective index over that of the substrate. The effective permittivity ($\varepsilon_{ff} = n_{eff}^2$) of the lossy transmission lines is 5.8, which is 1.6 times larger than the substrate permittivity ($\varepsilon_{sub} = 3.55$). Therefore, the low-loss sections are meandered to increase their phase delay per unit length to be identical to that of the lossy lines. The dimensions of the low loss lines are shown in Figure 4(a). The refractive index and Bloch impedance are shown in Figure 4(b). The Bloch impedance and $\mathrm{Re}(n_{eff})$ are very similar to that of the lossy transmission line, which suggests there is a good impedance and phase match.

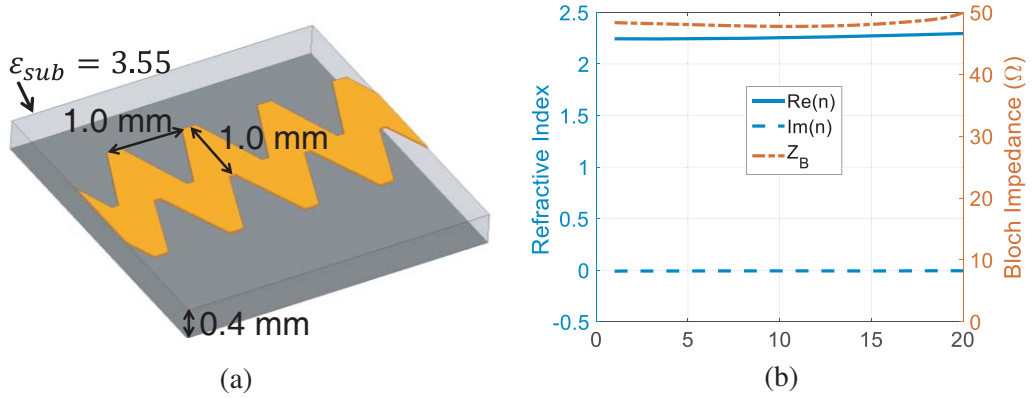

Figure 4. (a) Meandered microstrip line with refractive index equal to that of the lossy transmission lines. (b) Refractive index and Bloch impedance of the low-loss microstrip line.

3.3. Radiating Element

A UWB Vivaldi antenna array is chosen since Vivaldi radiators are notoriously simple to design and integrate onto a PCB [12]. The element spacing is 7.5 mm, which corresponds to $\lambda/2$ at 20 GHz at which point unwanted resonances in the active reflection coefficient typically appear in wideband arrays with tight element coupling. Therefore, the maximum operating frequency here is only 19 GHz. A myriad of other UWB antennas could also have been chosen, as there exists vast literature on this topic [13]. The Vivaldi antennas are designed within an infinitely periodic geometry as shown in Figure 5(a). A 50 Ω microstrip input line feeds a slot line with a 0.14 mm gap at the feed. The slot line is exponentially tapered over a 15 mm longitudinal distance to provide an impedance match to the wave impedance of free space (376 Ω). The 2 parallel, x-directed metallic rods with 2 mm diameters suppress unwanted cross-polarized radiation from the microstrip feed line. The simulated antenna performance when the infinite array points toward the broadside direction is shown in Figure 5(b). The active reflection coefficient is less than −3 dB from 2.7 GHz to 19 GHz. The maximum mismatch loss within the operating band of 6 GHz to 19 GHz is 2 dB at 12 GHz. The antennas have a relatively high mismatch loss compared to state-of-the art antenna arrays. Minimal time was spent optimizing the mismatch loss since the array has a poor radiation efficiency and is intended to be used in applications where low efficiencies are acceptable.

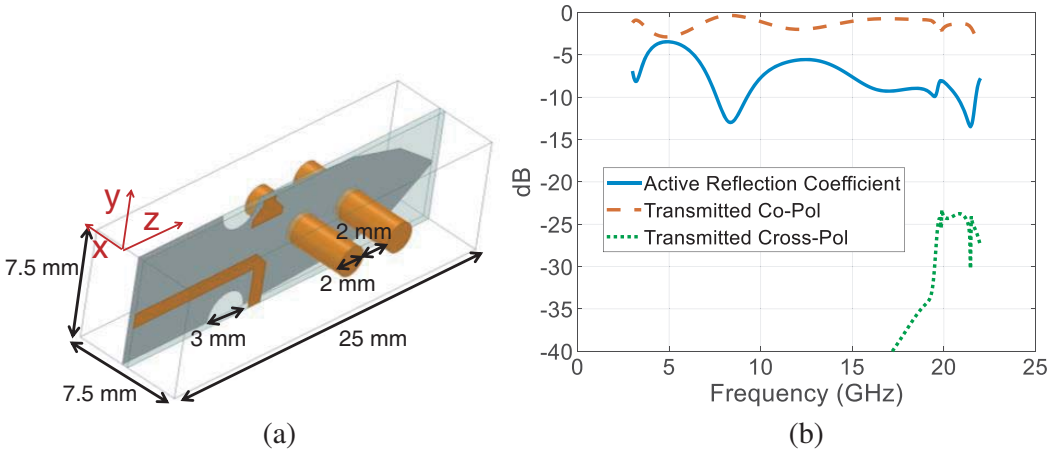

Figure 5. (a) Unit cell of the Vivaldi radiating element. The microstrip traces on the top side of the PCB are shown in orange, and the ground plane/Vivaldi radiator is shown in dark grey. (b) Active reflection coefficient, transmitted co-polarization, and transmitted cross-polarization of the unit cell when the infinite array points towards the broadside direction.

3.4. Overall Design

A 16×16 element array is designed to have a $1/e^2$ beamwidth of 30°. Given this aperture size, the minimum operating frequency is 6.5 GHz in accordance with Eq. (6). Each column card consists of a $1:16$ corporate power divider that feeds the variable loss transmissions lines. The transmission lines are then connected to UWB Vivaldi antenna radiators. These PCB column cards are connected to a PCB feed card that contains an identical $1:16$ power divider and lossy transmission lines. This ensures the 256 radiating elements have a radially symmetric excitation in accordance with Eq. (3). The corporate power dividers employ 3-stage Wilkinson power dividers for good impedance match and isolation. The PCBs are connected together using end-launch SMP connectors. Five terminated dummy elements are placed at all edges of the array as shown in Figure 6. This ensures that the embedded element patterns of the Vivaldi radiators are close to that of an infinite array.

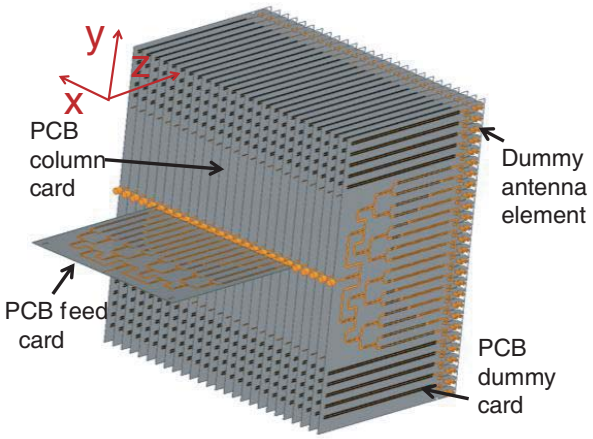

Figure 6. Antenna array with 5 dummy elements on each side to minimize edge effects.

The lossy line lengths at the edges of each card are shortened to increase the number of parts that can fit on a PCB panel, which reduces cost. Simulations suggest that this minimally impacts performance. Furthermore, 1 mm gaps in the resistive ink are placed every 5 mm along each lossy line to improve the reliability of the screen printing, fabrication process. The gaps in the resistive sheets

also do not have a significant impact on performance.

The entire array is too large to simulate with a full-wave solver using the available computational resources. Therefore, the performance of the array is estimated by multiplying the transmission coefficients of the various components (corporate power dividers, lossy transmission lines, low loss transmission lines, Vivaldi antenna elements). This assumes there is a good impedance match between each section up to the Vivaldi antennas. The radiation patterns assume the Vivaldi antennas have an element pattern identical to that of an infinite array. The radiation efficiency and directivity vs. frequency are shown in Figure 7(a). As expected the radiation efficiency reduces as the frequency is increased. The ripple in the radiation efficiency is primarily due to mismatch loss of the Vivaldi antennas and the insertion loss of 1 : 16 corporate power dividers. The 3 dB and 10 dB full beamwidths are shown in Figure 7(b). The array has a 10 dB full beamwidth of $35° \pm 5°$ and directivity of 20 dB $\pm$ 1.5 dB over 6.5 GHz–19 GHz (3 : 1 bandwidth ratio). As the frequency is reduced below 6.5 GHz, the lossy transmission lines are too short to absorb significant power. Therefore the aperture is more uniformly illuminated below 6.5 GHz, which leads to a frequency-dependent directivity below the minimum operating frequency. The radiation patterns in the E, H, and diagonal planes ($\phi = 45°$) are shown in Figure 8. The patterns are nearly identical from 6.5 GHz to 19 GHz, which agrees well with theory. The patterns have a cross-polarization below 30 dB in all three planes. It should be noted that simulations of the transmission lines and radiating elements assume an infinite array environment, which is known as the local periodicity assumption. This assumption leads to some discrepancy between the calculated and measured aperture field distributions. Experience suggests that this discrepancy is small though.

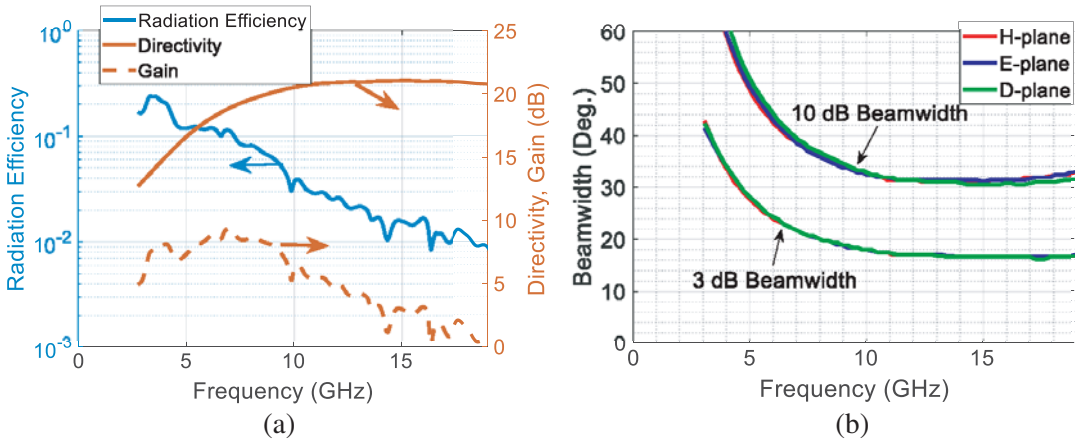

Figure 7. (a) Calculated directivity (right axis) and radiation efficiency (left axis) vs. frequency. (b) Calculated full beamwidth vs. frequency.

4. MEASUREMENTS

The prototype antenna is fabricated and measured. The printed circuit boards are constructed using standard double sided photolithography techniques on 0.4 mm thick Rogers 4003 boards. The resistive paste is screen printed onto the PCB. Two different views of the fabricated antenna are shown in Figure 9. The front of the antenna is shown in Figure 9(a). The Vivaldi arrays with perpendicular rods can be seen in the inset. Figure 9(b) shows the back of the array. The top of the feed card can be clearly seen which includes the black resistive paste along the lossy transmission lines. A white 3D printed casing properly aligns all of the PCB cards. This 3D printed casing is screwed to a black slotted metal frame around the outside to simplify mounting to external structures.

The measured 10 dB and 3 dB beamwidths in the E- and H-planes at different frequencies are shown in Figure 10(a). There is generally good agreement between measurements and calculations, which validates the underlying theory. However, there is a significant amount of ripple in the measured data. The measured gain in the broadside direction is shown in Figure 10(b). The measured radiation

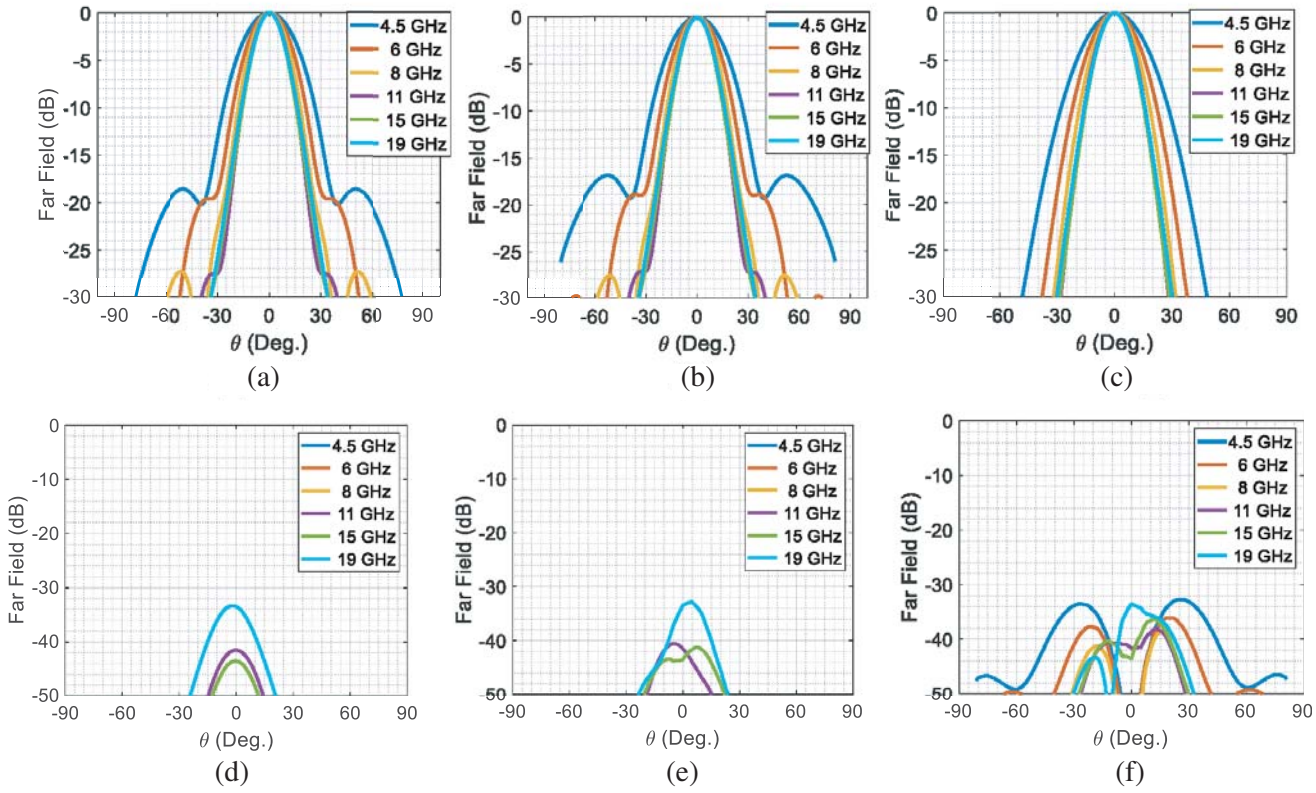

Figure 8. Calculated co-polarized radiation patterns in the (a) H-plane, (b) E-plane and (c) D-plane ($\phi = 45°$). Calculated cross-polarized radiation patterns in the (d) H-plane, (e) E-plane and (f) D-plane ($\phi = 45°$).

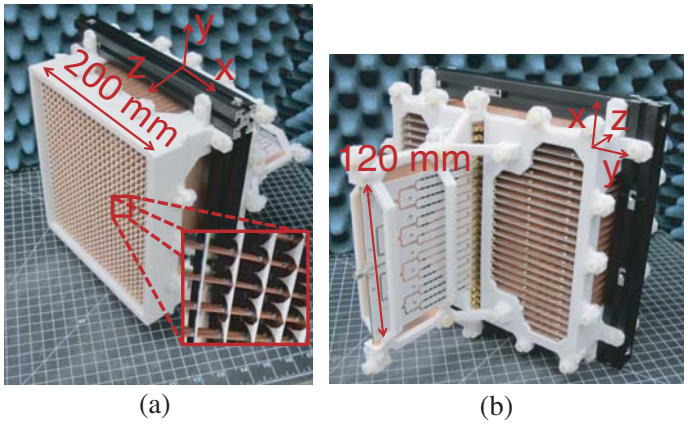

Figure 9. (a) and (b) Two different views of the fabricated prototype. The inset of (a) shows a zoomed in view of the wideband rod-loaded Vivaldi radiators located at the antenna aperture.

patterns in the E- and H-planes are shown in Figures 11(a) and (b), respectively. The first observation is the extremely high sidelobes, especially at the higher operating frequencies. Unfortunately, these unexpectedly high sidelobes make the current antenna unusable from a practical standpoint.

The theorized source of this unwanted radiation is from the corporate power divider feeding the lossy microstrip lines. It is well known that microstrip lines have radiative losses when they are bent.

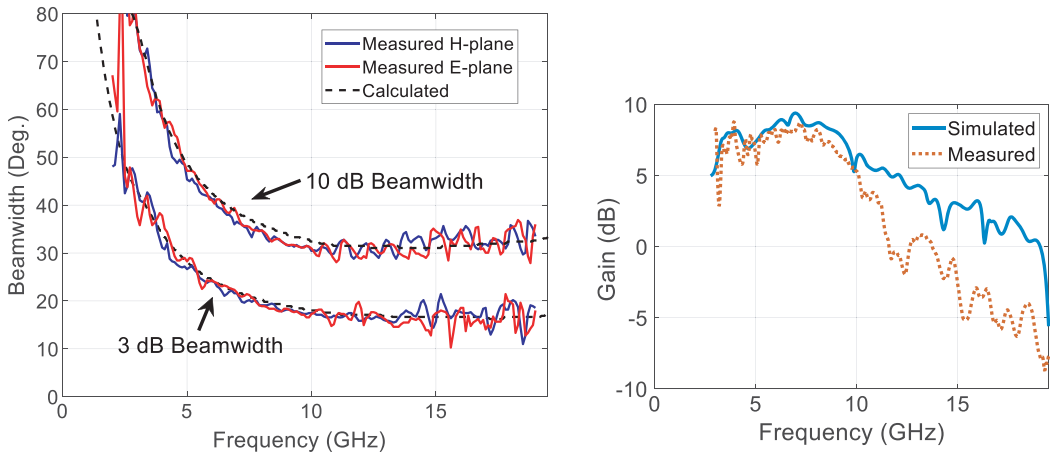

Figure 10. (a) Measured and predicted 10 dB and 3 dB beamwidths. (b) Measured and simulated gain in the broadside direction vs. frequency.

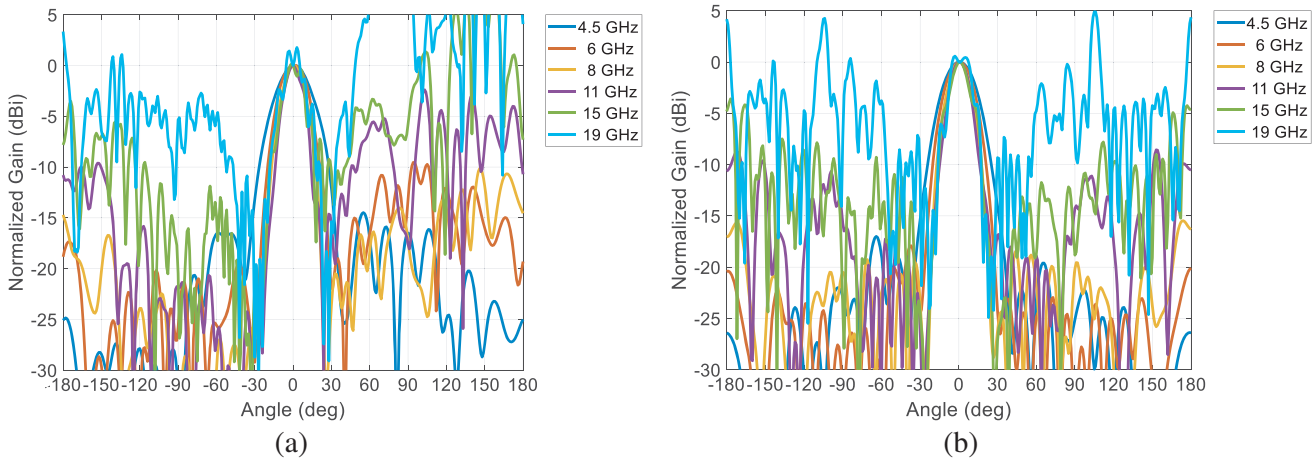

Figure 11. (a) and (b) Measured radiation patterns at various frequencies in the E- and H-planes, respectively.

Nevertheless, microstrip traces are often used because they are easy to fabricate and are low cost. The radiation from microstrip traces is typically low compared to radiation from the aperture, and therefore this radiation does not have a significant effect on the pattern for most antennas. However, the particularly lossy antenna reported here has a low radiation efficiency. Figure 12 plots the simulated fraction of incident power radiated by the aperture and corporate power dividers. The corporate power dividers actually radiate more power than the aperture over much of the designed bandwidth. The measured sidelobes are particularly high at $\theta > 90°$ in the E-plane. This is the region seen by the corporate power divider on the input feed card, which provides additional evidence that power divider radiation is the source of high sidelobes. As a point of reference, the normal direction of the input feed card is $\theta = 90°$ in the E-plane. Unfortunately, radiation from the corporate power divider was not properly considered before the array was fabricated, which led to this poor performance. In the future, a stripline geometry should be used to eliminate unwanted radiation from the corporate power divider. It is expected that a stripline based designed would have measured sidelobes much closer to simulation. Regrettably, time and budgetary constraints made it unfeasible to build a second version of the array using a stripline feed network.

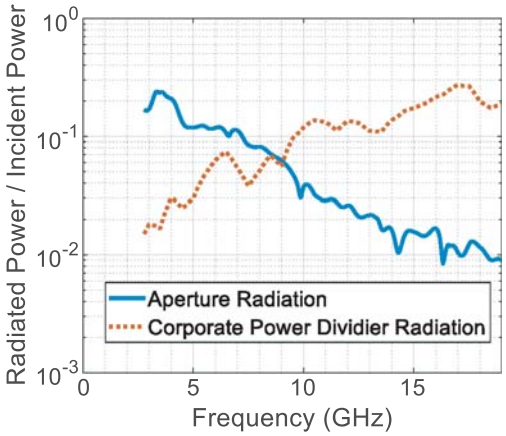

Figure 12. Simulated fraction of incident power radiated from the aperture and corporate power dividers. Above 10 GHz, unwanted radiation from the microstrip traces on the corporate power divider significantly exceeds the desired radiation from the Vivaldi antennas. This leads to large sidelobes and ripple in the measured patterns.

5. SUMMARY

A new method of designing UWB feed antennas with uniform beamwidths is reported. Resistively loaded transmission lines are systematically designed to generate the necessary frequency dependent loss for realizing a Gaussian amplitude taper across an arbitrarily large frequency range. A particularly nice feature of this approach is once the transmission line geometry is designed, the radiated beamwidth can be easily customized for a given application without requiring additional full-wave simulations. Furthermore, the cross-polarized radiation is inherently low (below 30 dB in simulation). The limitations of this approach are the resistively loaded transmission lines require long lengths for UWB antennas, which leads to a bulky antenna. In addition the radiation efficiency is low, especially for UWB designs. Measured beamwidths agree well with simulations, which provides validation for the reported theory. However, the fabricated antenna has significant radiation from the microstrip traces in the feed network. This radiation leads to large ripple in the radiation patterns and high sidelobes. In the future, a stripline based topology should eliminate unwanted radiation from the feed network so that the measured radiation patterns agree more closely with simulation.

ACKNOWLEDGMENT

The authors would like to thank Thomas Pemberton for his help in measuring the antenna.

REFERENCES

1. Kildal, P.-S., "Artificially soft and hard surfaces in electromagnetics," *IEEE Trans. on Antennas and Propagation*, Vol. 38, No. 10, 1537, 1990.
2. Goldsmith, P. F., "Quasi-optical techniques," *Proceedings of the IEEE*, Vol. 80, 1729–1747, 1992.
3. Chang, L.-C. T. and W. D. Burnside, "An ultrawide-bandwidth tapered resistive TEM horn antenna," *IEEE Trans. on Antennas and Propagation*, Vol. 48, No. 12, 1848, 2000.
4. Akgiray, A., S. Weinreb, W. A. Imbraile, and C. Beaudoin, "Circular quadruple-ridged flared horn achieving near-constant beamwidth over multioctave bandwidth: Design and measurements," *IEEE Trans. on Antennas and Propagation*, Vol. 61, No. 3, 1099, 2013.
5. Olsson, R., P.-S. Kildal, and S. Weinreb, "The Eleven antenna: A compact low-profile decade bandwidth dual polarized feed for reflector antennas," *IEEE Trans. on Antennas and Propagation*, Vol. 54, No. 2, 368, 2006.

6. Yang, J., X. Chen, N. Wadefalk, and P.-S. Kildal, "Design and realization of a linearly polarized Eleven feed for 1–10 GHz," *IEEE Antennas and Wireless Propagation Letters*, Vol. 8, 64, 2009.
7. Gawande, R. and R. Bradley, "Towards an ultra wideband low noise active sinuous feed for next generation radio telescopes," *IEEE Trans. on Antennas and Propagation*, Vol. 59, No. 6, 1945, 2011.
8. Bruni, S., A. Neto, and F. Marliani, "The ultrawideband leaky lens antenna," *IEEE Trans. on Antennas and Propagation*, Vol. 55, No. 10, 2642, 2007.
9. Ivashina, M. V., O. Iupikov, R. Maaskant, W. A. V. Cappellen, and T. Oosterloo, "An optimal beamforming strategy for wide-field surveys with phased-array-fed reflector antennas," *IEEE Trans. on Antennas and Propagation*, Vol. 59, No. 6, 1864, 2011.
10. Eleftheriades, G. V., A. K. Iyer, and P. C. Kremer, "Planar negative refractive index media using periodically L-C loaded transmission lines," *IEEE Trans. on Microwave Theory and Techniques*, Vol. 50, No. 12, 2702, 2002.
11. Pozar, D. M., *Microwave Engineering*, John Wiley & Sons, 2009.
12. Schaubert, D. H., S. Kasturi, A. O. Boryssenko, and W. M. Elsallal, "Vivaldi antenna arrays for wide bandwidth and electronic scanning," *European Conference on Antennas and Propagation*, Edinburgh, UK, 2007.
13. Kindt, R. and J. Logan, "Benchmarking ultrawideband phased antenna arrays: Striving for clearer and more informative reporting practices," *IEEE Antennas and Propagation Magazine*, Vol. 60, No. 3, 34, 2018.